THE JOURNAL OF BIOLOGICAL CHEMISTRY
Vol. 278, No. 24, Issue of June 13, pp. 21493–21501, 2003
Printed in U.S.A.

Molecular and Functional Characterization of the Melastatin-related Cation Channel TRPM3*

Received for publication, January 28, 2003, and in revised form, March 28, 2003
Published, JBC Papers in Press, April 2, 2003, DOI 10.1074/jbc.M300945200

Christian Grimm‡§¶, Robert Kraft‡¶, Sophie Sauerbruch‡, Günter Schultz‡, and Christian Harteneck‡‖

From the ‡Institut für Pharmakologie, Universitätsklinikum Benjamin Franklin, Freie Universität Berlin, Thielallee 69-73 and the §Fachbereich Biologie, Chemie, Pharmazie, Freie Universität Berlin, Takustraβe 3, Berlin 14195, Germany

Proteins of the mammalian TRP (transient receptor potential) family form a heterogenous group of cation channels important for cellular Ca^{2+} signaling and homeostasis. Here we present the full-length sequence of TRPM3, a member of the melastatin-like subfamily (TRPM) of TRP channels. TRPM3 expression was found in human kidney and brain. HEK293 cells transiently transfected with TRPM3 showed a constitutive Ca^{2+} and Mn^{2+} entry. Whole-cell patch clamp experiments confirmed the spontaneous activity of TRPM3 and revealed permeability ratios P_{Ca}/P_{Na} of 1.57 and P_{Na}/P_{Cs} of 0.75. In cell-attached patches, spontaneous inward and outward currents were observed. At negative membrane potentials and in the presence of either 140 mM Cs^+, 140 mM Na^+, or 100 mM Ca^{2+} in the pipette solution, the single channel conductance levels were 133, 83, and 65 pS, respectively. The Ca^{2+} entry in TRPM3-expressing HEK293 cells increased during treatment with hypotonic extracellular solution. The reduction of extracellular osmolarity was accompanied by cell swelling, suggesting volume-regulated activity of TRPM3. From its function and expression in human kidney, we propose a role of TRPM3 in renal Ca^{2+} homeostasis.

Proteins of the transient receptor potential (TRP)[1] superfamily form cation channels in the plasma membrane. They comprise a diverse group of ion channels that have been associated with a variety of cellular functions. According to structural and sequence similarities between individual TRP proteins, three subfamilies are distinguished: the classic TRPC, the vanilloid-like TRPV, and the melastatin-like TRPM subfamilies (1, 2). Nearly all members of the first two subfamilies have been characterized as Ca^{2+}-permeable channels, playing an important role in cellular Ca^{2+} homeostasis and/or signaling. Whereas the functional characterization of TRPM proteins is much more incomplete, recent studies implicate a particular structural and functional diversity within this group.

The eight known members of the TRPM subfamily can be subdivided into four groups according to their amino acid identity (3, 4). These subgroups are formed by the following pairs: TRPM1 (melastatin) and TRPM3 (KIAA1616), TRPM2 (TRPC7 or LTRPC2) and TRPM8 (Trp-p8), TRPM4 and TRPM5 (MTR1), and TRPM6 (ChaK2) and TRPM7 (TRP-PLIK or ChaK1). The first member of the TRPM subfamily that was functionally characterized was TRPM7 (5). It is a Ca^{2+}- and Mg^{2+}-permeable channel, inhibited by intracellular Mg^{2+} and ATP (6, 7). The inactivation of TRPM7 is coupled to the hydrolysis of phosphatidylinositol 4,5-biphosphate (8). Unlike other members of the TRP family, TRPM7 and TRPM6 have C-terminal regions with sequence similarity to the atypical kinase family, the alpha-kinase family (9). Despite the lack of functional data, TRPM6 has been associated with Mg^{2+} transport, because mutations in TRPM6 cause a disorder with a defect in intestinal magnesium absorption (10, 11). TRPM2 and TRPM8 have been shown to function as Ca^{2+}-permeable channels activated in the presence of intracellular ADP-ribose (12–14) and during exposure to lowered temperature or menthol (15, 16), respectively. Expression of TRPM4 induced spontaneous Ca^{2+} entry in HEK293 cells (17). However, a second TRPM4 form (TRPM4b) that includes additional 174 amino acids at the N-terminal end was characterized as a Ca^{2+}-activated channel specific for monovalent cations (18). TRPM5 expression was recently found in taste receptor cells, and its heterologous expression revealed that it is activated by depletion of intracellular Ca^{2+} stores (19). Melastatin (TRPM1), the founding member of the TRPM subfamily, was first detected in melanoma tumor cell lines, and its down-regulation was correlated with the potential for melanoma metastasis (20). It was, therefore, suggested to be a tumor-suppressor protein (20–22). Heterologously expressed melastatin was shown to induce Ca^{2+} entry, and the channel appeared to be regulated by a cytoplasmic isoform (17).

Here we report the molecular structure and expression pattern of TRPM3, the closest relative to melastatin. Functional studies on TRPM3-transfected HEK293 cells revealed Ca^{2+} entry and cation currents activated by reduction of extracellular osmolarity.

EXPERIMENTAL PROCEDURES

cDNA Cloning and Sequence Determination—The whole sequence of EST AA745664 from human kidney (American Type Culture collection, Rockville, MD) was determined and used to select synthetic oligonucleotides as primers for nested RACE reactions, which were always used in combination with the adaptor primers AP1 and AP2 of the human fetal brain and kidney Marathon-Ready cDNA (Clontech, Palo Alto, CA). In a first round of nested 3′-RACE reactions, we were able to amplify a 3.4-kb DNA fragment using NSKR125 and NSKR126 (Table

* This work was supported by the Deutsche Forschungsgemeinschaft and Fonds der Chemischen Industrie. The costs of publication of this article were defrayed in part by the payment of page charges. This article must therefore be hereby marked "*advertisement*" in accordance with 18 U.S.C. Section 1734 solely to indicate this fact.

The nucleotide sequence(s) reported in this paper has been submitted to the GenBank™/EBI Data Bank with accession number(s) AJ505026.

¶ Both authors contributed equally to this work.

‖ To whom correspondence should be addressed. Tel.: 49-30-8445-1825; Fax: 49-30-8445-1818; E-mail: hartenek@zedat.fu-berlin.de.

[1] The abbreviations used are: TRP, transient receptor potential; TRPC, classic TRP; TRPV, vanilloid-like TRP; TRPM, melastatin-like TRP; EST, expressed sequence tag; RACE, rapid amplification of cDNA ends; GFP, green fluorescent protein; RT, reverse transcription; NPPB, 5-nitro-2-(3-phenylpropylamino)benzoic acid; MIC, Mg^{2+}-inhibited cation; $NMDG^+$, *N*-methyl-D-glucamine.

TABLE I
Sequences of synthetic oligonucleotides used

NSKR125	5′-CATCATACCCAGCACCAAAGACCCCCATAG-3′
NSKR126	5′-CCTGGGGGCCTGCAGAACTTTGAACT-3′
NSKR159	5′-CATGGAAAGGGAAGGAGTGGTTGAT-3′
NSKR160	5′-ATATCATCCTCCATTCCCAGCAGTTTCA-3′
NSKR161	5′-GCAGAAGAACCAGAGAAGCCCACAAAG-3′
NSKR304	5′-TTATACTGAATAAAGAGGATGCTCTGCAG-3′
NSKR305	5′-TACTGAATAAAGAGGATGCTCTGCAGGG-3′
NSKR330	5′-CACCATGCCAGAGCCGTGGGGGACGGTT-3′
NSKRT734	5′-TTGGGGCCGAAGAGGTTGTGGTA-3′
NSKRT735	5′-CAAAGCCATGTATGTGCGAGTATC-3′

I). The fragment was subcloned in the TOPOpCR2.1 vector (Invitrogen, Groningen, The Netherlands). For determination of the 5′-end, NSKR159 and NSKR160 (see Table I) were used in nested RACE reactions to amplify a 2.2-kb fragment. In a second round of 3′-RACE reactions, NSKR125 and NSKR161 (see Table I) were able to amplify fragments of 2.0 kb containing the 3′-untranslated regions and poly(A) stretches. The fragments of TRPM3 were subsequently subcloned to result in TRPM3 with an open reading frame of 1325 amino acid residues. The sequence data have been submitted to the GenBank™ data base under accession number AJ505026.

A plasmid construct coding for the entire open reading frame was generated by subsequent subcloning of the three fragments. For subcloning in the expression vector TOPOpcDNA3.1/V5 (Invitrogen, Groningen, The Netherlands), the plasmids were linearized by digestion with *Bam*HI. After isolation of the linearized plasmid DNA, the full coding sequence of TRPM3 was amplified by using NSKR330/304 (see Table I) to result in expression of wild-type TRPM3. For expression as fusion protein with C-terminal V5-antibody epitope and His_6 tag or GFP, we used oligonucleotides eliminating the endogenous stop codon NSKR330/NSKR305 (see Table I) for amplification. The PCR was performed under the following conditions. An initial denaturation (94 °C for 2 min) was followed by seven PCR cycles (94 °C for 30 s; 68 °C for 300 s) and a final extension step (72 °C for 7 min). The PCR reaction mixture contained 30 pM of each primer, 0.5 μg of template DNA, 200 μM of each dNTP, and 2.6 units of polymerase-enzyme mixture (Expand HF, Roche Applied Science, Indianapolis, IN). For expression as YFP fusion protein, the coding sequence of YFP was subcloned in-frame by using *Not*I and *Avr*II restriction sites. DNA for transient transfection was prepared using anion exchange columns (Qiagen, Hilden, Germany).

All cDNA inserts of PCR reactions were sequenced on both strands using ABI Prism BigDye terminator cycle sequencing kits and an ABI Prism 377 DNA sequencer (Applied Biosystems, Weiterstadt, Germany). Subsequent analysis of sequence data was performed with the Lasergene software package (Lasergene, Madison, WI).

Cell Culture and Transfections—HEK293 cells were cultured in Earle's minimal essential medium (Biochrom, Berlin, Germany), supplemented with 10% fetal calf serum (Biochrom), 100 units ml^{-1} penicillin, 100 $\mu g\ ml^{-1}$ streptomycin under 5% CO_2 atmosphere at 37 °C. Cells were plated in 85-mm dishes onto glass coverslips and transiently transfected with 1.5–2 μg of DNA and 5 μl of FuGENE 6 transfection reagent (Roche Applied Science, Indianapolis, IN) in 95 μl of Opti-MEM medium vector (Invitrogen, Groningen, The Netherlands) 2 days later. Fluorescence measurements and electrophysiological studies were carried out 2–3 days after transfection.

Northern Blot and RT-PCR—Northern blot hybridization was performed as described previously (23). Briefly, DNA fragments (0.65-, 0.8-, 0.9-, and 1.4-kb fragments after digestion of TRPM3 in pCR2.1 with Bsp120I, *Xba*I, and *Xho*I) were radiolabeled according to a standard random-priming procedure using [α-^{32}P]dATP in parallel reactions; unincorporated nucleotides were removed. Total RNA was extracted from various mouse tissues using TRIzol reagent (Invitrogen, Groningen, The Netherlands) according to the standard protocol. For Northern blot hybridization, 10 μg of total RNA per lane was loaded on a denaturing formamide/formaldehyde-agarose gel. After electrophoresis, RNA was transferred on a charged nylon membrane (Tropilon Plus, Applied Biosystems, Weiterstadt, Germany) by capillary transfer. RNA was fixed on the membrane surface by UV light and by heating in an incubator at 80 °C for 2 h. The blots, mouse multiple tissue Northern and human multiple tissue Northern (12-lane (tissues), Clontech, Palo Alto, CA), were hybridized with a mixture of all labeling reactions. Hybridization and washing steps were performed with Ultrahyb hybridization mix (Ambion, Huntingdon, UK) according to the standard protocol. Post-hybridization wash steps were performed at 55 °C beginning with 2× SSC and 0.1% (W/V) SDS and ending up with 0.2× SSC plus 0.1% (w/v) SDS. The blots were exposed for 7–14 days with an intensifying screen on Kodak X-Omat AR films. RT-PCR analysis of human tissues was performed using multiple cDNA panels I and II (Clontech) as template and the oligonucleotides NSKRT734/735 (see Table I) in a standard PCR reaction. Products were separated in a 1% agarose gel, and the DNA/ethidium bromide-dependent fluorescence was documented using a video camera system.

Western Blot—For generation of polyclonal rabbit antisera, we analyzed the delineated protein sequence and selected a synthetic peptide with probability to be immunogenic. The synthetic peptide from position 807 to 821 (CQEKEAEEPEKPTKE) was synthesized with an N-terminal cysteine for coupling to KLH. Following coupling three rabbits were immunized. Antiserum from day 90 was tested. The whole antiserum was isolated at day 100, and the specific IgG fraction was isolated by affinity column purification (Pineda Antikörper-Service, Berlin, Germany).

Human membrane extracts (Sigma, Deisenhofen, Germany) and membrane fractions of bovine and mouse tissues and transfected cells were separated on a 6% polyacrylamide gel (24). The proteins were transferred on nitrocellulose membranes, and the TRPM3 protein was detected by incubating the membrane with antibody solution at 4 °C overnight. The next day, the membranes were washed with TBST buffer, and the bound antibody was detected using an ECL Advance Western Blotting Detection kit (Amersham Biosciences, Freiburg, Germany).

Fluorescence Measurements—$[Ca^{2+}]_i$ measurements in single cells were carried out using the fluorescence indicator fura-2 in combination with a monochromator-based imaging system (T.I.L.L. Photonics, Martinsried, Germany) attached to an inverted microscope (Axiovert 100, Zeiss, Oberkochen, Germany). HEK293 cells were loaded with 4 μM fura-2-AM (Fura-2/AM, Molecular Probes Europe, Leiden, The Netherlands) supplemented with 0.01% Pluronic F127 for 60 min at 37 °C in a standard solution containing 138 mM NaCl, 6 mM KCl, 1 mM $MgCl_2$, 2 mM $CaCl_2$, 5.5 mM glucose, and 10 mM HEPES (adjusted to pH 7.4 with NaOH). Coverslips were then washed in this buffer for 20 min and mounted in a perfusion chamber on the microscope stage. Osmolarity effects were studied in a solution with 88 mM instead of 138 mM NaCl containing 0, 100, and 200 mM mannitol resulting in osmolarities of 200, 300, and 400 mosmol $liter^{-1}$, respectively. The osmolarity of the solutions was measured using a freezing point depression osmometer (Roebling, Berlin, Germany). For $[Ca^{2+}]_i$ measurements, fluorescence was excited at 340 and 380 nm. After correction for the individual background fluorescence, the fluorescence ratio F_{340}/F_{380} was calculated. Fluorescence quenching by Mn^{2+} entry was studied using the fura-2 isosbestic excitation wavelength at 360 nm, and the emitted light was monitored using the same filter system as for $[Ca^{2+}]_i$ measurements. In all experiments, transfected cells were identified by their YFP- or GFP-fluorescence at an excitation wavelength of 480 nm.

The relative cell volume was spectroscopically determined using two-dimensional fura-2 fluorescence images at the isosbestic wavelength (23). The integral fluorescence intensity of an area that contained the whole cell at all times was divided by the integral fluorescence of a spot within the cell. This fluorescence ratio is reciprocal to the cytosolic fura-2 concentration and thus reflects the cell volume. The confocal images of transfected cells were acquired with a laser scanning microscope (LSM 510, Zeiss, Oberkochen, Germany) equipped with a krypton/argon ion laser.

Patch Clamp Measurements and Data Analysis—Membrane currents were measured in the whole-cell and cell-attached configuration of the patch clamp technique. Currents were recorded using an EPC-7 amplifier (HEKA, Lambrecht, Germany), subsequently low pass-filtered at 1 kHz, digitized with a sampling rate of 5 or 10 kHz, and analyzed using pCLAMP software (version 7.0, Axon Instruments, Burlingame, CA). The pipette resistance varied between 2 and 5 MΩ. Whole-cell currents were elicited by voltage ramps from −100 mV to +100 mV (400-ms duration) applied every 5 s from a holding potential of 0 mV.

Pipettes for whole-cell recordings were filled with a solution composed of 130 mM $CsCH_3O_3S$, 10 mM CsCl, 2 or 5 mM $MgCl_2$, 10 mM 1,2-bis(2-aminophenoxy)ethane-*N*,*N*,*N*′,*N*′-tetraacetic acid and 10 mM HEPES (pH 7.2 with CsOH). The bath solution contained 140 mM NaCl, 2 mM $CaCl_2$, 1 mM $MgCl_2$, 10 mM glucose, and 10 mM HEPES (pH 7.4 with NaOH). For Na^+-free conditions, Na^+ was replaced with 140 mM *N*-methyl-D-glucamine ($NMDG^+$).

Relative cation permeabilities were calculated by Equations 1 and 2,

$$P_{Na}/P_{Cs} = ([Cs^+]_o/[Na^+]_o)\exp(\Delta E_{rev}F/RT) \quad \text{(Eq. 1)}$$

and

$$P_{Ca}/P_M = ([M^+]_o/4[Ca^{2+}]_o)\exp(\Delta E_{rev}F/RT)[1 + \exp(E_{rev,Ca}F/RT)] \quad \text{(Eq. 2)}$$

where E_{rev} is the reversal potential of whole-cell currents measured in the divalent cation-free, Na^+-containing bath solution ($E_{rev,Na}$), the divalent cation-free, Cs^+-containing solution ($E_{rev,Cs}$), and the solution containing 20 mM Ca^{2+} ($E_{rev,Ca}$). ΔE_{rev} is a change in the reversal potential ($E_{rev,Na} - E_{rev,Cs}$ or $E_{rev,Ca} - E_{rev,M}$), M^+ is either Cs^+ or Na^+, F is the Faraday constant, R is the gas constant, and T is the absolute temperature. The ion concentrations were corrected for the respective activity coefficients (0.76 for 140 mM NaCl, 0.73 for 140 mM CsCl, and 0.66 for 20 mM $CaCl_2$).

To test the effects of hypotonic solution, cells were initially bathed in a solution containing 80 mM sodium gluconate, 10 mM NaCl, 2 mM $CaCl_2$, 1 mM $MgCl_2$, 10 mM glucose, 10 mM HEPES, and 100 mM mannitol (pH 7.4 with NaOH); 100 mM mannitol was then removed to reduce osmolarity from 300 to 200 mosmol $liter^{-1}$. In some experiments 5-nitro-2-(3-phenylpropylamino)benzoic acid (NPPB, RBI, Deisenhofen, Germany) was applied during hypotonic treatment. Whole-cell currents were measured using the perforated-patch technique with amphotericin B (0.25 mg ml^{-1}, Sigma).

Single-channel currents were continuously measured at different pipette potentials. The corresponding membrane potentials for cell-attached patches were calculated by Equation 3,

$$V_m = V_c - V_p + V_L \quad \text{(Eq. 3)}$$

where V_m is the membrane potential, V_c is the resting potential of the cell, and V_L is the junction potential. To obtain $V_c = 0$ mV, the bath solution contained 140 mM KCl, 2 mM $CaCl_2$, and 1 mM $MgCl_2$ (pH 7.4). Pipettes were either filled with 130 mM $CsCH_3O_3S$ (cesium methane sulfonate), 10 mM CsCl, and 10 mM HEPES (pH 7.4) or with 130 mM sodium gluconate, 10 mM NaCl, and 10 mM HEPES (pH 7.4) or with 100 mM $CaCl_2$ and 10 mM HEPES (pH 7.4). Values for V_L were calculated using pCLAMP software (version 7.0). Single-channel amplitudes at different V_m values were calculated from current traces of 2–4 s using amplitude histograms fitted to Gaussian functions.

All pooled data from fluorescence measurements are given as means ± S.E. from n experiments containing 20–40 cells, unless otherwise noted. All pooled data from patch-clamp experiments are expressed as means ± S.E. from n cells.

RESULTS

Primary Structure of TRPM3—Searching the EST subset of the GenBank™ data base, we found an expressed sequence tag (EST) from human kidney (EST AA745664) with sequence homologies to the N-terminal sequence of melastatin. We determined the sequence of the entire clone (798 bp) obtained from ATCC. On the basis of this sequence, we were able to clone the complete cDNA of the protein, which showed homologies to the previously identified mouse EST AA038185 (1, 4) and was, therefore, designated TRPM3 (Fig. 1*A*). The putative open reading frame starts at nucleotide 245 of the consensus sequence (Fig. 1*B*). The in-frame stop codon (nucleotide 176) in the upstream 5′-untranslated region argues for the translational start at position 245, although the score for prediction of the start methionine is low. The presence of the motif, (W/F)LX_3–(F/L/I)XK(R/K)EC(V/I/S)X_{12-24}CXCG, downstream at position 63 confirmed the cloning of the entire cDNA of TRPM3 with the correct start position (Fig. 1*C*). This motif is present in nearly all mammalian (except for TRPM5), *Drosophila melanogaster*, and *Caenorhabditis elegans* members of the TRPM subfamily.

Tissue Distribution of TRPM3—Tissue distribution of TRPM3 was studied by Northern blot and RT-PCR analyses. Different multiple tissue Northern blots were hybridized and resulted in signals from mRNAs in human kidney (Fig. 2*A*). The Northern blot results were confirmed by RT-PCR analysis. We found signals in cDNA of kidney, brain, ovaria, and pancreas (Fig. 2*B*). Northern blot analysis of multiple mouse tissues resulted in strong signals in brain, whereas in kidney no signal could be detected (Fig. 2*C*).

For detection of TRPM3 protein, an antibody was generated by immunization of rabbits. The antisera were tested using lysates and membrane fractions of transiently transfected HEK293 cells (Fig. 3*A*). The expressed protein detected by antibody showed an apparent molecular mass of about 160 kDa, which is in good agreement with the calculated molecular mass (157 kDa). The specificity of the antibody reaction was verified by incubating parallel lanes with the antibody in the presence of the peptide used for immunization (Fig. 3*A*). The antiserum was subsequently used to detect TRPM3 expression in extracts from bovine, human, and mouse tissues (Fig. 3*B*). In mouse brain, proteins with molecular masses of around 130 and 220 kDa were detected by using the antiserum (Fig. 3*B*). In mouse kidney, TRPM3 was not detectable, whereas in bovine kidney, human brain, and human kidney, a clear signal with an apparent molecular mass of about 160 kDa was detected (Fig. 3*B*). Although the TRPM3 cDNA codes for the protein expressed in bovine kidney, human brain, and human kidney, the proteins detected in mouse brain are probably products from alternatively spliced transcripts. In summary, TRPM3 is expressed in bovine and human kidney but not in mouse kidney.

TRPM3 Mediates Constitutive Ca^{2+} Entry—To study cellular distribution and function of heterologously expressed TRPM3, the cDNA was subcloned as wild-type and fusion-protein constructs in eukaryotic expression vectors. Subcellular distribution of TRPM3 in transiently transfected cells was investigated by confocal fluorescence microscopy. Prominent signals of TRPM3 were detected in the intracellular compartments of the cells, but slight signals were also seen in regions of the plasma membrane (Fig. 4*A*).

Functional studies were performed in fura-2-loaded and transiently transfected or in co-transfected HEK293 cells. In fluorescence quench experiments using 1 mM Mn^{2+}, a rapid reduction of fluorescence intensity was observed in TRPM3-transfected cells but not in YFP-transfected control cells (Fig. 4*B*). To verify the specificity of this TRPM3-mediated Mn^{2+} entry, we used substances known to block cation channels of the TRP family. Gd^{3+} (100 μM, Fig. 4*B*) and La^{3+} (100 μM, data not shown) completely inhibited the Mn^{2+} influx, whereas SK&F-96365 (100 μM, data not shown) did not significantly block the quench. The cytosolic Ca^{2+} concentration, $[Ca^{2+}]_i$, was increased in TRPM3-transfected but not in YFP-transfected HEK293 cells (Fig. 4*C*). This elevated $[Ca^{2+}]_i$ level was evoked by Ca^{2+} entry, indicated by the decrease in fluorescence ratios in the absence of extracellular Ca^{2+} (Fig. 4*C*).

Permeation Properties of TRPM3—In accordance with the spontaneous Ca^{2+} and Mn^{2+} entry, whole-cell patch clamp experiments revealed constitutively activated cation currents in TRPM3-expressing cells. The exchange of Na^+ for the large cation $NMDG^+$ in the bath solution resulted in a clear decrease in inward currents in TRPM3-transfected HEK293 cells (Fig. 5*A*). The $NMDG^+$-sensitive inward current was −8.2 ± 1.3 pA $picofarad^{-1}$ at −80 mV (n = 58) using a Ca^{2+}-free, Mg^{2+}-containing (2 or 5 mM) pipette solution. In YFP-transfected control cells, the $NMDG^+$-sensitive current was −1.8 ± 0.3 pA $picofarad^{-1}$ at −80 mV (n = 13). The current-voltage relationship of the current of spontaneously active TRPM3 showed no clear rectification and a reversal potential (E_{rev}) of −7.6 ± 0.6 mV (n = 58). Application of the cation channel blocker Gd^{3+} (100 μM) completely suppressed inward and outward currents (n = 4, Fig. 5*A*), whereas external SK&F-96365 (100 μM) had no significant effect (n = 3, Fig. 5*A*). To study the selectivity of the current of constitutively active TRPM3 in transfected cells, we replaced the standard extracellular solution containing Na^+, Ca^{2+}, and Mg^{2+} by solutions containing only one of the cations $NMDG^+$, Na^+, Cs^+, Ca^{2+}, or Mg^{2+}. In Na^+-containing bath solution the removal of divalent cations induced a slight increase of inward (Fig. 5*B*) and outward currents (not shown). The reversal potentials, however, were similar with −9.0 ± 1.5 mV (n = 4) and −9.8 ± 2.2 mV (n = 4) in the presence and

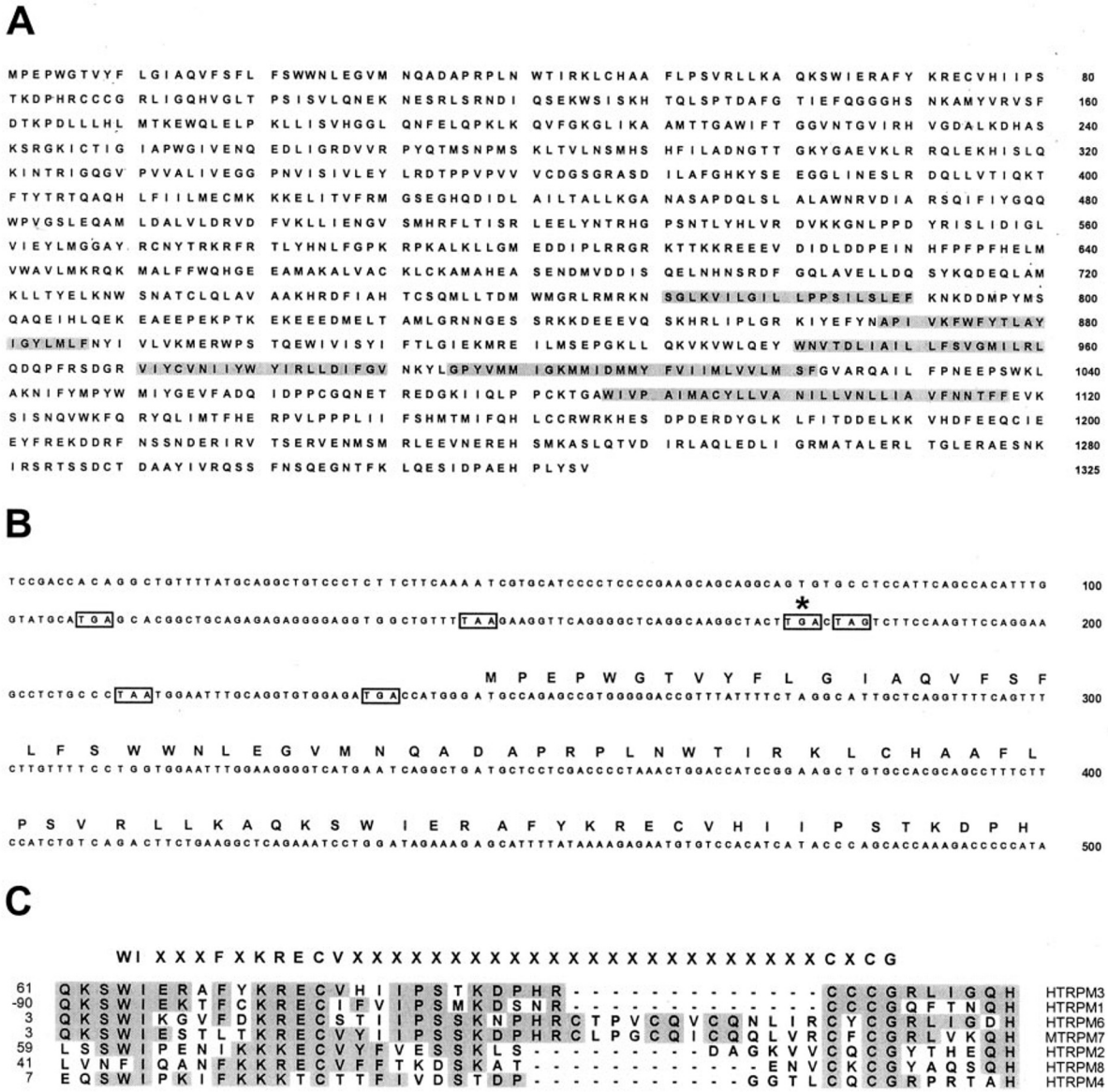

FIG. 1. **Sequence of TRPM3.** *A*, protein sequence encoded by the cDNA of TRPM3 is shown. Sequences of the putative transmembrane domains are marked by *shading*. *B*, the 500-bp fragment contains the 5′-untranslated region with stop codons (*boxed*), the translational start position (*first M*), and N-terminal coding region of TRPM3. The stop codon at position 176 (*asterisk*) is in-frame to the proposed translational start position (at nucleotide 245). *C*, N-terminal sequences of TRPM3 (GenBank™ number AJ505026) and published sequence data of TRPM6 (GenBank™ number AF448232), TRPM7 (GenBank™ number NM_017672), TRPM2 (GenBank™ number M64722), TRPM8 (GenBank™ number AY090109), and TRPM4 (GenBank™ number AF497623) were aligned. Sequence of TRPM1 (GenBank™ number AF071787) was delineated from the 5′-untranslated region of the published cDNA entry. All shown mammalian TRPM proteins code for a highly conserved exon of 60–80 bp, which can also be detected in TRPM channels of *D. melanogaster* and *C. elegans* (data not shown). Amino acids conserved in the majority of the compared sequences are *shaded*. The resulting consensus sequence is shown *above* the alignment.

absence of divalent cations, respectively. Under divalent-free conditions, the exchange of Na^+ for Cs^+ further increased inward currents and shifted E_{rev} to -3.1 ± 2.5 mV ($n = 4$). In experiments with 20 mM Ca^{2+}, we added 100 mM $NMDG^+$ to the bath solution to obtain normal osmolarity. The measured E_{rev} was -24.8 ± 3.1 mV ($n = 4$) under these conditions. With 100 mM external Ca^{2+}, hyperpolarizing potentials evoked inward currents of nearly similar amplitude and noise as observed in the presence of 140 mM Na^+ or Cs^+ (Fig. 5, *B* and *C*). With 100 mM Mg^{2+}, inward current amplitudes were smaller than in standard bath solution but significantly increased compared with the $NMDG^+$ solution (Fig. 5*D*), indicating permeability for Mg^{2+}. From the shifts of E_{rev} during subsequent application of Na^+ (140 mM), Cs^+ (140 mM), and Ca^{2+} (20 mM) we calculated permeability ratios according to Equations 1 and 2. Permeability ratios of constitutively active TRPM3 were 1.14 ± 0.10 for P_{Ca}/P_{Cs}, 0.74 ± 0.09 for P_{Na}/P_{Cs}, and 1.57 ± 0.31 for P_{Ca}/P_{Na}.

Single Channel Properties of TRPM3—Because whole-cell recordings revealed spontaneous mono- and divalent cation currents, we performed cell-attached patch experiments in TRPM3-transfected, unstimulated HEK293 cells. After performing the cell-attached configuration, all cells were initially tested for several minutes at membrane potentials between -40 and -80 mV (according to Equation 3). Under these conditions, single channel amplitudes between 2 and 8 pA were observed in 7 out of 39 TRPM3-transfected and in 0 out of 11 YFP-transfected HEK293 cells. The amplitude of these currents was largely independent of the ionic composition of the extracellular pipette solution. Examples of spontaneous channel activity in the presence of extracellular Cs^+ and Ca^{2+} are shown in Fig. 6 (*A* and *B*, respectively). With a pipette solution

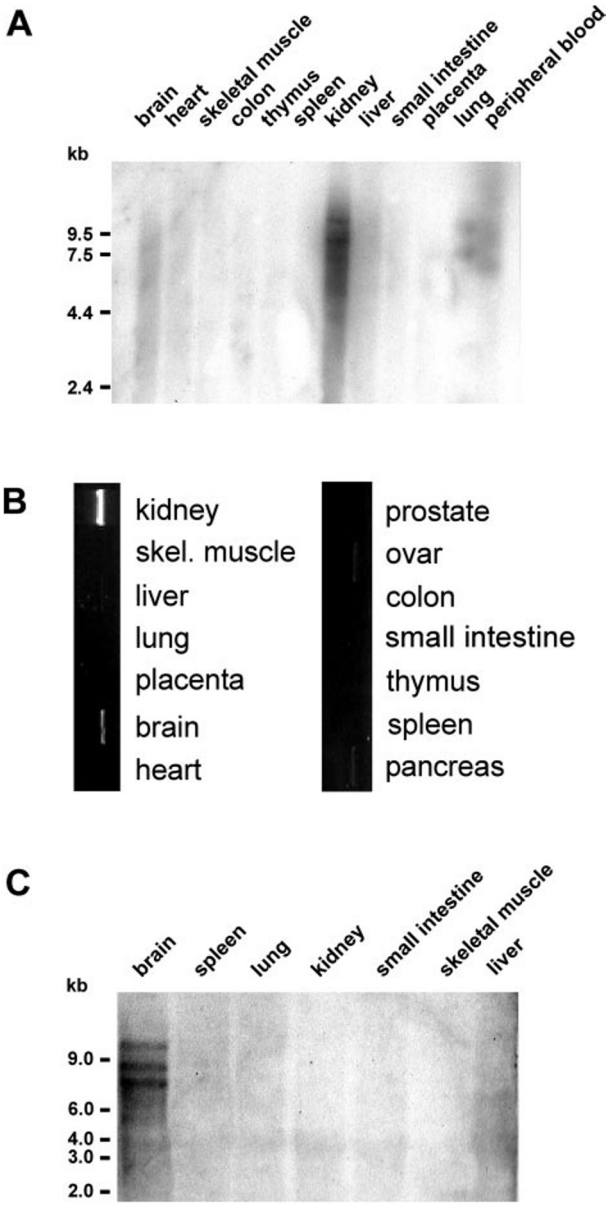

FIG. 2. **Analysis of tissue distribution of TRPM3 mRNA.** *A*, Northern blot analysis of human tissues was performed as described under "Experimental Procedures." Signals resulting from TRPM3 probes are visible in the *lane* of mRNA extracted from human kidney. *B*, multiple tissue cDNA panels from human were used as template to amplify DNA fragments specific for TRPM3. In reactions performed from kidney, brain, pancreas, and ovaria cDNAs a specific 1316-bp fragment was amplified. *C*, Northern blot analysis of murine tissues was performed as described under "Experimental Procedures." Signals resulting from TRPM3 probes are visible in the *lane* of mRNA extracted from mouse brain.

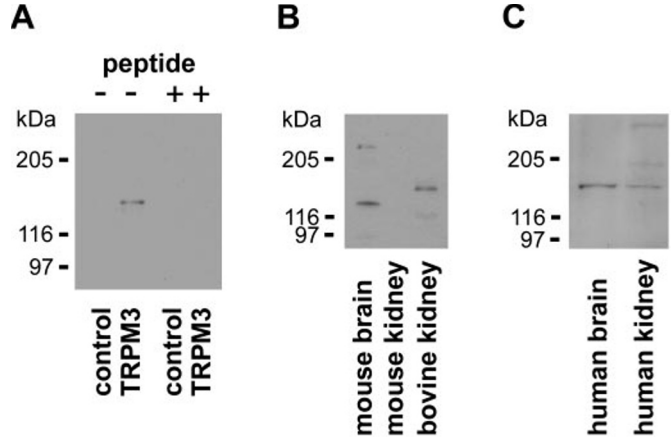

FIG. 3. **Immunodetection of TRPM3 protein.** Western blots of membrane proteins from TRPM3-transfected HEK293 cells and tissue extracts are shown. The specific protein-antibody interaction was visualized by chemiluminescence using a specific anti-IgG rabbit antibody (1:20,000). *A*, membrane proteins from non-transfected control cells and TRPM3-transfected cells were loaded as described under "Experimental Procedures." The immobilized TRPM3 protein was detected by incubation of the nitrocellulose membrane with a specific anti-TRPM3 antibody (1:2,000). To block the specific reaction of the antibody, membrane proteins were coincubated with the peptide (0.4 mg/ml) used for immunization. *B*, membrane proteins from mouse brain, mouse kidney, and bovine kidney immobilized on nitrocellulose membranes were incubated with a specific anti-TRPM3 antibody (1:2,000). *C*, membrane proteins from human brain and kidney immobilized on nitrocellulose membranes were incubated with a specific anti-TRPM3 antibody (1:1,000).

containing either 140 mM Cs^+/10 mM Cl^- or 100 mM $CaCl_2$, single-channel currents displayed an E_{rev} close to 0 mV (Fig. 6*C*), indicating activity of a nonselective cation channel. From current amplitudes at membrane potentials of −60 and +60 mV, the respective chord conductance levels were 133 and 118 pS with 140 mM extracellular Cs^+ ($n = 2$) and 83 and 97 pS with 140 mM extracellular Na^+ ($n = 3$). With 100 mM extracellular Ca^{2+} and at a membrane potential of −60 mV, the chord conductance was 65 pS ($n = 2$), whereas analysis of channel activity at membrane potentials > +30 mV revealed no stable opened and closed states.

Regulation of TRPM3 by Changes in Extracellular Osmolarity—To resolve the activation mechanism of TRPM3, we tested known stimuli of TRP-homologous channels in fluorescence quench experiments or by measuring the cytosolic Ca^{2+} concentration $[Ca^{2+}]_i$ of HEK293 cells. The dependence of TRPM3 activity on the filling state of intracellular Ca^{2+} stores was tested by the application of thapsigargin (2 μM) inducing passive depletion of these stores. Regulation of TRPM3 by G-protein-coupled receptors was studied by hormonal stimulation with histamine in cells co-transfected with TRPM3 and histamine H_1 receptor or with carbachol activating endogenously expressed muscarinic receptors in HEK293 cells. Neither thapsigargin nor hormonal stimulation of transfected cells resulted in any change of the Mn^{2+} entry (data not shown). From its expression in the kidney, we supposed a modulation of TRPM3 activity by changes in extracellular osmolarity. To test this hypothesis, we used a standard buffer supplemented with 0, 100, and 200 mM mannitol to achieve solutions with 200, 300, and 400 mosmol $liter^{-1}$, respectively. Application of hypotonic extracellular solution (200 mosmol $liter^{-1}$) produced a rise of $[Ca^{2+}]_i$ in TRPM3-transfected (Fig. 7*A*) compared with nontransfected control cells (Fig. 7*B*) and a strong swelling in both TRPM3-transfected (Fig. 7*A*) and control cells (Fig. 7*B*). The increase in cell volume reversed during application of normal osmolarity. Although these volume changes were rapidly induced after rinsing the cells with hypo- and isotonic solutions, the respective increase and decrease in $[Ca^{2+}]_i$ started 10–30 s later. On the other hand, application of hypertonic extracellular solution (400 mosmol $liter^{-1}$) resulted in a decrease in $[Ca^{2+}]_i$ in TRPM3-transfected cells (Fig. 7*C*), whereas YFP-transfected cells showed no response (data not shown). The hypotonic Ca^{2+} response in TRPM3-transfected cells was suppressed by transient application of EGTA-containing solution (200 mosmol $liter^{-1}$) or application of isotonic solution (Fig. 7*C*). From this we suggest a volume-dependent regulation of TRPM3 in HEK293 cells.

A member of the TRPV subfamily, TRPV4 (OTRPC4, TRP12), was shown to be regulated by changes in osmolarity

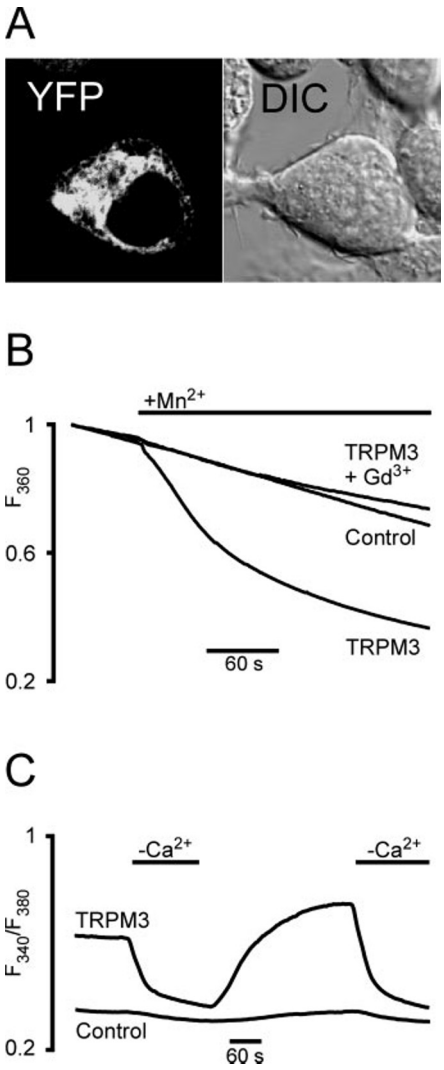

FIG. 4. **TRPM3 induces constitutive Ca^{2+} and Mn^{2+} influx in HEK293 cells.** *A*, confocal image of the subcellular localization of TRPM3-YFP transiently transfected in HEK293 cells (*YFP*). The same cell is shown using differential interference contrast optics (*DIC*). *B*, addition of 1 mM Mn^{2+} to the standard solution rapidly decreased fluorescence at 360 nM in fura-2-loaded, TRPM3-YFP-transfected (n = 6) but not in YFP-transfected control cells (n = 5). The TRPM3-mediated Mn^{2+} quench was inhibited by application of 100 μM Gd^{3+} at the start of the experiment (n = 3). *C*, changes in $[Ca^{2+}]_i$ are depicted by fluorescence ratios F_{340}/F_{380} of fura-2-loaded HEK293 cells. TRPM3-YFP-transfected (n = 4) and YFP-transfected control cells (n = 3) were subsequently exposed to isotonic solutions containing either 2 mM Ca^{2+} or 1 mM EGTA. All *traces* are means of independent experiments.

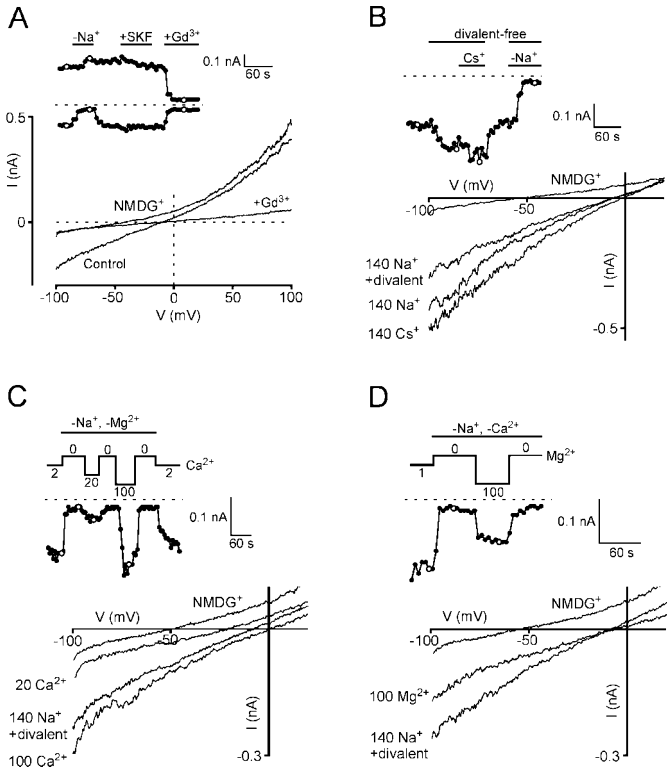

FIG. 5. **Spontaneous whole-cell currents in TRPM3-expressing cells.** All currents were recorded during voltage ramps from −100 to +100 mV. Each *inset* shows the corresponding time course of currents at −80 (*A–D*) and +80 mV (*A*) obtained from the voltage ramps. In all experiments, exchange of external cations for $NMDG^+$ nearly completely suppressed inward currents, indicative for cation-permeable ion channels. *A*, the cation channel blocker SK&F-96365 (100 μM) had no effect, whereas Gd^{3+} (100 μM) blocked both inward and outward currents. *B*, removal of external divalent cations from the Na^+-containing bath solution and exchange of Na^+ for Cs^+ increased inward current amplitudes. Exchange of extracellular Na^+ for Cs^+ shifted the reversal potential of currents to more positive values. *C*, addition of 20 mM Ca^{2+} to a $NMDG^+$-containing bath solution and exchange of $NMDG^+$ for 100 mM Ca^{2+} increased inward currents and shifted reversal potentials to more positive values. *D*, exchange of $NMDG^+$ for 100 mM Mg^{2+} increased inward currents and shifted reversal potentials to more positive values.

and cell swelling in a similar manner (23, 25–27). Besides its sensitivity to La^{3+} and Gd^{3+}, TRPV4-mediated Ca^{2+} entry has further been described to be blocked by ruthenium red (1 μM) (23). Therefore, in side-by-side experiments, we measured fluorescence of TRPV4-GFP- and TRPM3-YFP-transfected, fura-2-loaded HEK293 cells. The decrease in external osmolarity from 300 to 200 mosmol $liter^{-1}$ induced an increase in $[Ca^{2+}]_i$ in both transfections with higher peak responses in TRPV4-transfected cells (Fig. 7*D*). All Ca^{2+} signals were suppressed by application of an EGTA-containing solution, indicating Ca^{2+} entry (data not shown). Addition of 1 μM ruthenium red to hypotonic solution clearly suppressed TRPV4-mediated responses but only slightly affected TRPM3-mediated Ca^{2+} signals (Fig. 7*D*). Individual cells expressing TRPV4 showed a typical variability in the latency of response after hypotonic challenge (23). In TRPM3-transfected cells this latency appeared more uniformly (Fig. 7*D*).

To test whether osmotic stimuli also modulate TRPM3-mediated currents, we applied conventional whole-cell and perforated-patch techniques to TRPM3-transfected HEK293 cells. Configuration of conventional whole-cell recording resulted in currents that were mostly insensitive to decreased (200 mosmol $liter^{-1}$) osmolarity (data not shown). In perforated-patch experiments, however, five of eleven cells tested clearly responded to hypotonic solution (Fig. 8). To minimize the contribution of endogenous swelling-activated Cl^- currents ($I_{Cl,swell}$), the external $[Cl^-]$ was reduced to 16 mM, and the Cl^- channel blocker NPPB (50 μM) was applied in some cases. Under these conditions, application of hypotonic solution resulted in a reversible activation of inward and outward currents. Because the extracellular medium contained 90 instead of 140 mM Na^+ in the standard bath solution, the E_{rev} of the currents was shifted to more negative potentials (−18 ± 3 mV; n = 5). In contrast, hypotonic stimulation of YFP-transfected HEK293 cells either had no effect on whole-cell currents or led to the induction of $I_{Cl,swell}$. In solutions with reduced $[Cl^-]$, these Cl^- currents could be identified by a shift of E_{rev} to more positive voltages and by sensitivity to NPPB (data not shown).

DISCUSSION

We have cloned and characterized TRPM3, a member of the TRPM subfamily of channel proteins (2), which is predomi-

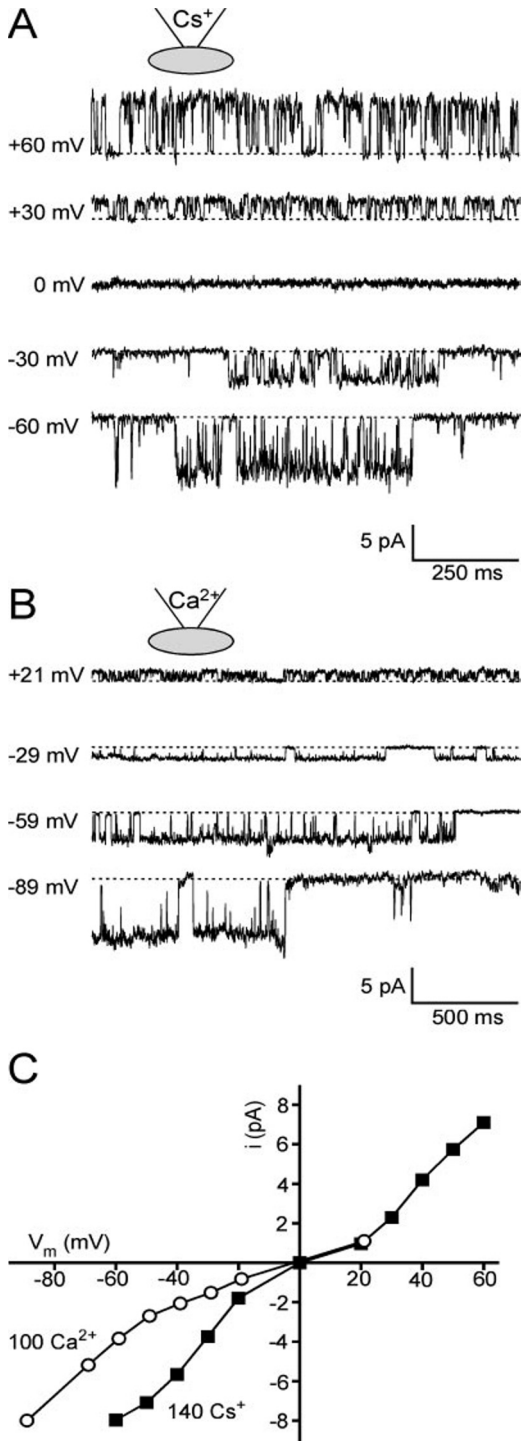

FIG. 6. **Single-channel properties of TRPM3 in cell-attached patches.** Examples of spontaneous currents in cell-attached patches from TRPM3-YFP-expressing HEK293 cells at the indicated membrane potentials. The extracellular pipette solution contained either 140 mM Cs^+ and 10 mM Cl^- (*A*) or 100 mM $CaCl_2$ (*B*). The bath solution contained 140 mM KCl to bring to zero the resting membrane potential. *C*, current-voltage relationship for single-channel currents from the experiments shown in *A* and *B*.

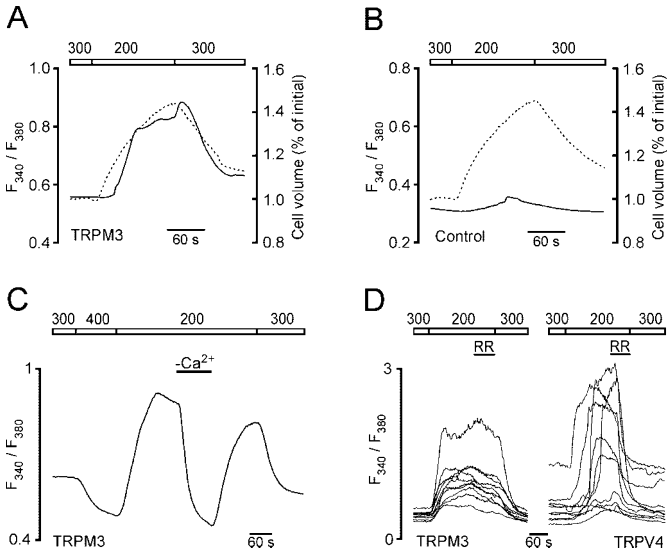

FIG. 7. **Ca^{2+} responses in TRPM3-expressing cells upon osmotic stimulation.** Changes in $[Ca^{2+}]_i$ are depicted by fluorescence ratios F_{340}/F_{380} of fura-2-loaded HEK293 cells. The relative cell volume (*dotted line*) and $[Ca^{2+}]_i$ (*straight line*) in TRPM3-YFP-expressing cells (*A*) and non-transfected control cells (*B*) was measured during application of hypotonic solution. The relative cell volume was calculated from the fura-2 fluorescence at the isosbestic point (see "Experimental Procedures"). *Traces* are means from 12 cells (TRPM3) and 10 cells (control) from three experiments. *C*, TRPM3-YFP-transfected cells were subsequently exposed to solutions with osmolarities of 300, 400, 200, and 300 mosmol $liter^{-1}$. During application of the hypotonic solution (200 mosmol $liter^{-1}$), 2 mM Ca^{2+} was exchanged for 1 mM EGTA. The *trace* is the mean of seven independent experiments containing 20–40 cells. *D*, comparison of TRPM3- and TRPV4-mediated $[Ca^{2+}]_i$ signals in representative cells (each $n = 10$) exposed to hypotonic solution and the effect of 1 μM ruthenium red (*RR*). HEK293 cells were transfected with TRPM3-YFP or TRPV4-GFP.

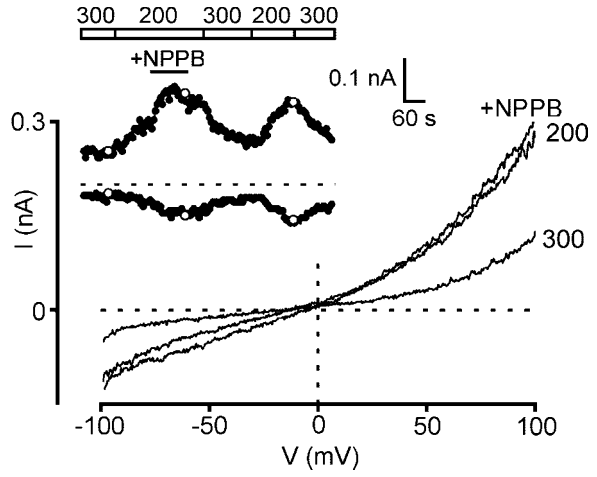

FIG. 8. **TRPM3-mediated whole-cell currents during hypotonic stimulation.** Currents were recorded during voltage ramps from −100 to +100 mV using the perforated-patch technique. A TRPM3-YFP-transfected cell was repetitively exposed to solutions with osmolarities of 300 and 200 mosmol $liter^{-1}$. Application of NPPB (50 μM), a blocker of volume-regulated Cl^- currents, had no effect on currents during hypotonic stimulation. The *inset* shows the time course of the currents at −80 and +80 mV throughout the experiment.

nantly expressed in human kidney. TRPM3 forms constitutively active, Ca^{2+}-permeable cation channels when expressed in HEK293 cells. The activity of TRPM3 is increased by reduction of extracellular osmolarity.

A partial amino acid sequence of TRPM3 has previously been reported (1), showing highest similarity with melastatin (TRPM1), the founding member of the TRPM subfamily (4). In the present study we completed the sequence of TRPM3 resulting in a protein of 1325 amino acids. TRPM3 and melastatin are both homologous to TRPM6 and TRPM7, which are TRP channels sharing a C-terminal enzymatic domain. However, we were unable to identify any sequence motif in the C terminus of TRPM3 arguing for enzymatic activity. Using the HEK293 expression system, we detected constitutive activity of TRPM3. Expression of TRPM1 and TRPM7 in HEK293 cells has been

shown to mediate spontaneous Ca^{2+} entry (8, 17). In contrast to the spontaneous activity of TRPM1, TRPM3, and TRPM7, some other members of the subfamily, *i.e.* TRPM2, TRPM4, and TRPM8, require intra- or extracellular signals, such as elevation of intracellular ADP-ribose, intracellular Ca^{2+}, or exposure to cold temperature and cooling agents to induce cation currents or Ca^{2+} influx after overexpression in HEK293 or Chinese hamster ovary cells (12, 13, 15, 16, 18).

Analysis of constitutive ion currents in TRPM3-transfected HEK293 cells revealed good accordance between properties in whole cells and cell-attached patches. Most remarkably, whole-cell currents were characterized by a similar noise independent of the extracellular cation species, *i.e.* Ca^{2+}, Na^+, or Cs^+. The respective single channels showed relative high conductance levels of 65, 83, and 133 pS when exposed to extracellular Ca^{2+}, Na^+, and Cs^+, respectively. In whole-cell recordings, the removal of divalent cations resulted only in a slight increase of monovalent cation currents. Furthermore, intracellular perfusion with Ca^{2+}-free, BAPTA-containing solution was sufficient to evoke TRPM3-mediated currents. From this and the stable channel activation with high extracellular [Ca^{2+}] we suggest a largely Ca^{2+}-independent regulation of TRPM3. In contrast, the activity of another TRPM protein, TRPM4b, which is endogenously expressed in HEK293 cells, has been shown to depend on increased $[Ca^{2+}]_i$ (18). Therefore, we exclude a contribution of endogenous Ca^{2+}-activated cation currents to the TRPM3 activity. Furthermore, TRPM3 activation was observed in the presence of 2 or 5 mM $[Mg^{2+}]_i$. At these concentrations, a complete inhibition of the TRPM3-related channel TRPM7 has been reported (5). Endogenously expressed Mg^{2+}-inhibited cation (MIC) channels in RBL and Jurkat T cells have been shown to be sensitive to $[Mg^{2+}]_i$ in a similar manner (28). Because endogenous MIC currents in HEK293 (5) are completely blocked by $[Mg^{2+}]_i \geq 2$ mM in the absence of ATP,[2] a contribution to TRPM3-mediated currents can be excluded.

With respect to its relative permeability for Ca^{2+} (P_{Ca}/P_{Cs} = 1.14, P_{Ca}/P_{Na} = 1.57) and its single-channel conductance for monovalent cations (between 83 and 133 pS at negative membrane potentials), TRPM3 can be further compared with other members of the melastatin-like TRP subfamily. TRPM2 has been shown to have a P_{Ca}/P_{Cs} of 0.67 (13) and a nearly linear current-voltage relationship with a single-channel conductance between 58 and 76 pS (12, 13). For the cold receptor TRPM8, permeability ratios P_{Ca}/P_{Na} of 0.97 (16) and 3.3 (15) have been reported. TRPM8 showed a single-channel conductance of 83 pS at positive membrane potentials but a pronounced outward rectification (15). Likewise, TRPM7-mediated currents displayed an outward rectification and single-channel conductance levels between 40 pS (5) and 105 pS (6). In summary, TRPM3 and the previously described TRPM2, TRPM7, and TRPM8 show a nearly similar Ca^{2+} permeability and a single-channel conductance of at least 40 pS. However, a pronounced rectification of currents as shown for TRPM7 and TRPM8 was not observed for TRPM3.

Despite some functional similarities between TRPM members regarding the structure of the channel pore, rather large differences in the activation properties led us to test for regulatory mechanisms of TRPM3 already described for members of other TRP subfamilies. TRPV4, a cation channel of the vanilloid-like TRP subfamily, was described as a sensor of extracellular osmolarity being activated upon hypotonic stimulation (23, 25). Indeed, we found an increase in Ca^{2+} influx when TRPM3-transfected HEK293 cells were exposed to lowered osmolarity. The pattern of TRPM3- and TRPV4-mediated Ca^{2+} responses, however, differed significantly: side-by-side experiments revealed a stronger Ca^{2+} influx in individual TRPV4-expressing cells but a more uniform delay of the response on hypotonic treatment in individual TRPM3-expressing cells. Furthermore, the inhibitor ruthenium red (1 μM) completely inhibited TRPV4-mediated Ca^{2+} signals but did not affect responses to hypotonic solution in TRPM3-transfected cells. In contrast to TRPM3, TRPV4 was shown to have a higher Ca^{2+} permeability (P_{Ca}/P_{Na}) and a lower single-channel conductance of 6.3 (23) and 35–60 pS (23, 29), respectively. A structural analysis of TRPM3 and TRPV4 revealed low sequence identity and no according sequence motif indicating a common osmolarity or cell-volume sensor. Interestingly, two other TRP channels, TRPV1 (VR1) and TRPM8, which both respond to changes in temperature (15, 16, 30) show only 21% sequence identity and quite divergent intracellular domains (16). It is up to now unclear, whether physical stimuli such as changes in cell volume and temperature act directly on TRPV and TRPM channels or induce an intracellular signal cascade leading to channel activation. Therefore, further functional studies may help to clear up the mechanism of osmotic regulation in both TRPM3 and TRPV4.

Northern blot and RT-PCR analyses of TRPM3 suggested an expression in human kidney and at lower level in human brain. In mouse brain, we found clearly distinct signals corresponding to mRNAs of different lengths. From this, we suggest the occurrence of differently spliced TRPM3 mRNAs. The absence of TRPM3 expression in mouse kidney was confirmed by Western blot analysis, whereas a specific TRPM3 signal was found in bovine and human kidney. The surprising absence of TRPM3 in mouse kidney raises the question of the physiological relevance in different species. Whereas in human and bovine kidney the osmotic regulation of TRPM3 suggests a role of this channel in renal Ca^{2+} homeostasis, its possible function in mouse remains unclear.

Acknowledgment—We thank I. Reinsch for technical assistance.

REFERENCES

1. Harteneck, C., Plant, T. D., and Schultz, G. (2000) *Trends Neurosci.* **23,** 159–166
2. Montell, C., Birnbaumer, L., Flockerzi, V., Bindels, R. J., Bruford, E. A., Caterina, M. J., Clapham, D. E., Harteneck, C., Heller, S., Julius, D., Kojima, I., Mori, Y., Penner, R., Prawitt, D., Scharenberg, A. M., Schultz, G., Shimizu, N., and Zhu, M. X. (2002) *Mol. Cell* **9,** 229–231
3. Clapham, D. E., Runnels, L. W., and Strübing, C. (2001) *Nat. Rev. Neurosci.* **2,** 387–396
4. Montell, C., Birnbaumer, L., and Flockerzi, V. (2002) *Cell* **108,** 595–598
5. Nadler, M. J., Hermosura, M. C., Inabe, K., Perraud, A. L., Zhu, Q., Stokes, A. J., Kurosaki, T., Kinet, J. P., Penner, R., Scharenberg, A. M., and Fleig, A. (2001) *Nature* **411,** 590–595
6. Runnels, L. W., Yue, L., and Clapham, D. E. (2001) *Science* **291,** 1043–1047
7. Hermosura, M. C., Monteilh-Zoller, M. K., Scharenberg, A. M., Penner, R., and Fleig, A. (2002) *J. Physiol.* **539,** 445–458
8. Runnels, L. W., Yue, L., and Clapham, D. E. (2002) *Nat. Cell Biol.* **4,** 329–336
9. Ryazanov, A. G., Ward, M. D., Mendola, C. E., Pavur, K. S., Dorovkov, M. V., Wiedmann, M., Erdjument-Bromage, H., Tempst, P., Parmer, T. G., Prostko, C. R., Germino, F. J., and Hait, W. N. (1997) *Proc. Natl. Acad. Sci. U. S. A.* **94,** 4884–4889
10. Schlingmann, K. P., Weber, S., Peters, M., Niemann Nejsum, L., Vitzthum, H., Klingel, K., Kratz, M., Haddad, E., Ristoff, E., Dinour, D., Syrrou, M., Nielsen, S., Sassen, M., Waldegger, S., Seyberth, H. W., and Konrad, M. (2002) *Nat. Genet.* **31,** 166–170
11. Walder, R. Y., Landau, D., Meyer, P., Shalev, H., Tsolia, M., Borochowitz, Z., Boettger, M. B., Beck, G. E., Englehardt, R. K., Carmi, R., and Sheffield, V. C. (2002) *Nat. Genet.* **31,** 171–174
12. Perraud, A. L., Fleig, A., Dunn, C. A., Bagley, L. A., Launay, P., Schmitz, C., Stokes, A. J., Zhu, Q., Bessman, M. J., Penner, R., Kinet, J. P., and Scharenberg, A. M. (2001) *Nature* **411,** 595–599
13. Sano, Y., Inamura, K., Miyake, A., Mochizuki, S., Yokoi, H., Matsushime, H., and Furuichi, K. (2001) *Science* **293,** 1327–1330
14. Hara, Y., Wakamori, M., Ishii, M., Maeno, E., Nishida, M., Yoshida, T., Yamada, H., Shimizu, S., Mori, E., Kudoh, J., Shimizu, N., Kurose, H., Okada, Y., Imoto, K., and Mori, Y. (2002) *Mol. Cell* **9,** 163–173
15. McKemy, D. D., Neuhausser, W. M., and Julius, D. (2002) *Nature* **416,** 52–58
16. Peier, A. M., Moqrich, A., Hergarden, A. C., Reeve, A. J., Andersson, D. A., Story, G. M., Earley, T. J., Dragoni, I., McIntyre, P., Bevan, S., and Patapoutian, A. (2002) *Cell* **108,** 705–715

[2] R. Kraft, unpublished observation.

17. Xu, X. Z., Moebius, F., Gill, D. L., and Montell, C. (2001) *Proc. Natl. Acad. Sci. U. S. A.* **98,** 10692–10697
18. Launay, P., Fleig, A., Perraud, A. L., Scharenberg, A. M., Penner, R., and Kinet, J. P. (2002) *Cell* **109,** 397–407
19. Perez, C. A., Huang, L., Rong, M., Kozak, J. A., Preuss, A. K., Zhang, H., Max, M., and Margolskee, R. F. (2002) *Nat. Neurosci.* **5,** 1169–1176
20. Duncan, L. M., Deeds, J., Hunter, J., Shao, J., Holmgren, L. M., Woolf, E. A., Tepper, R. I., and Shyjan, A. W. (1998) *Cancer Res.* **58,** 1515–1520
21. Hunter, J. J., Shao, J., Smutko, J. S., Dussault, B. J., Nagle, D. L., Woolf, E. A., Holmgren, L. M., Moore, K. J., and Shyjan, A. W. (1998) *Genomics* **54,** 116–123
22. Duncan, L. M., Deeds, J., Cronin, F. E., Donovan, M., Sober, A. J., Kauffman, M., and McCarthy, J. J. (2001) *J. Clin. Oncol.* **19,** 568–576
23. Strotmann, R., Harteneck, C., Nunnenmacher, K., Schultz, G., and Plant, T. D. (2000) *Nat. Cell Biol.* **2,** 695–702
24. Laemmli, U. K. (1970) *Nature* **227,** 680–685
25. Liedtke, W., Choe, Y., Marti-Renom, M. A., Bell, A. M., Denis, C. S., Sali, A., Hudspeth, A. J., Friedman, J. M., and Heller, S. (2000) *Cell* **103,** 525–535
26. Wissenbach, U., Bödding, M., Freichel, M., and Flockerzi, V. (2000) *FEBS Lett.* **485,** 127–134
27. Nilius, B., Prenen, J., Wissenbach, U., Bödding, M., and Droogmans, G. (2001) *Pflügers Arch.* **443,** 227–233
28. Kozak, J. A., Kerschbaum, H. H., and Cahalan, M. D. (2002) *J. Gen. Physiol.* **120,** 221–235
29. Watanabe, H., Vriens, J., Suh, S. H., Benham, C. D., Droogmans, G., and Nilius, B. (2002) *J. Biol. Chem.* **277,** 47044–47051
30. Caterina, M. J., Schumacher, M. A., Tominaga, M., Rosen, T. A., Levine, J. D., and Julius, D. (1997) *Nature* **389,** 816–824